



Formation and evolution of early-type galaxies

C. Chiosi and E. Merlin

Department of Physics & Astronomy "Galileo Galilei", Vicolo Osservatorio 2, I-35122, Padova, Italy, e-mail: [cesare.chiosi;emiliano.merlin]@unipd.it

Abstract. In this review, we present some recent results for NB-TSPH models of early type galaxies (ETGs) made of Dark and Baryonic matter according to the Λ -CDM model of the Universe. The models are framed in the quasi-monolithic or early hierarchical scenario. By means of fully hydrodynamical NB-TSPH simulations performed with the Padova code EvoL, we produce a number of self-similar models of ETGs for different initial total masses and over-densities with respect to the surrounding medium, and follow their evolution from the detachment from the linear regime and Hubble flow at $z \geq 20$ down to the stage of nearly complete assembly of the stellar content (at about $z \leq 1$ for all of them) and often to the present epoch ($z = 0$). We find a strong correlation between the total mass and/or over-density of the proto-haloes and the subsequent star formation histories (SFH). Massive ($M_{tot} \simeq 10^{13} M_{\odot}$) haloes experience a single, intense burst of star formation (with rates $\geq 10^3 M_{\odot}/\text{yr}$) at early epochs, consistently with observations, with a weak dependence on the initial over-density; intermediate mass ($M_{tot} \simeq 10^{11} M_{\odot}$) haloes have histories that strongly depend on their initial over-density; finally, low mass haloes ($M_{tot} \simeq 10^9 M_{\odot}$) always have erratic, burst-like star forming histories. The model galaxies have morphological, structural, and chemical properties resembling those of real galaxies. In addition to this, we try to cast light on the physical causes of the tight correlation between the mass in stars and the size of ETGs (the Mass-Radius Relation, MRR). We suggest that the MRR is the result of two complementary mechanisms: on one hand, the result of local physical processes, which fix the star mass and the radius of individual objects; on the other hand, the action of cosmological global, statistical principles, which shape the distribution of objects in the MR-plane. In the picture emerging from this study, *nature* seems to play the dominant role, whereas *nurture* has a secondary importance.

Key words. Galaxies: observational data – Galaxies: early types – Galaxies: formation and evolution – Galaxies: mass-radius relation

1. Introduction

In a Universe containing three main components in cosmic proportions: Dark Energy (DE, 70%), Dark Matter (DM, 25%), and Baryonic Matter + Neutrinos (BM, 5%), the formation and evolution of galaxies are among the hot topics of modern astrophysics. In brief the clas-

sical paradigm of galaxy formation (the ETGs, in particular) stands on the following prescription: the above composition of the Universe, the hierarchical clustering of DM+BM from small size bodies to large complexes under the action of gravity, hierarchical mergers of DM + BM haloes to form "visible galaxies" all over the Hubble time, according to which mas-

sive galaxies are the end product of repeated mergers and are in place only at rather recent times. However, the observational data are currently telling us a more complicated history because massive galaxies with mass of the order of $10^{12} M_{\odot}$ are detected at high redshift ($z \geq 5$). Over the years two competing scenarios for galaxy formation have been proposed: the Monolithic and the Hierarchical Scenarios both with a number possible variants.

Monolithic: massive ETGs form at high redshift by rapid collapse and undergo a single, prominent star formation episode, ever since followed by quiescence. Over the years this view has been changed to the so-called Revised Monolithic scheme: a great deal of the stars in massive ETGs are formed very early-on at high redshifts and the remaining ones at lower redshifts.

Hierarchical: massive ETGs are the end product of subsequent mergers of smaller subunits over time scales almost equal to the Hubble time. Complementary alternatives to this simple scheme are the Dry Mergers (fusion of gas-free galaxies to avoid star formation) and the Wet Mergers (the same but with some stellar activity).

For long time the preference has gone to the hierarchical scheme that was considered the reference frame for any theory of ETGs formation (the massive ones in particular). The success of this theory is mainly due to the achievements obtained in modelling the large scale gravitational structures like the large scale structure of Universe itself, galaxy groups, and galaxy clusters. However its extension to individual galaxies is still a matter of debate and often in conflict with modern observational data. In any case, the potential capability of the monolithic-like mode has not been fully explored.

Therefore, in this review we concentrate on the models obtained with the Revised Monolithic scheme by Merlin et al. (2012) and shortly report on how they are able to reproduce current observational data for ETGs. First, we summarize the state of the art of the input physics of NB-TSPH galaxy models, second we highlight the role of the initial density and total mass of the system in determining the

kind of star formation that takes place in ETGs, third we report on the large scale structure of model galaxies, and finally we present highlight the physical origin of the MRR according to the study by Chiosi et al. (2012).

Before describing our galaxy models, we like to recall that any theory of galaxy formation and evolution must obey two different groups of constraints, i.e. those provided by the Scale Relations and the pattern of properties of the Stellar Content of the galaxies. Since all this has been widely discussed in literature, we do not need to address these topics in detail here. The only point we like to note is that the observational data may trace the SFH of a galaxy of different morphological type. In some way the kind of star formation occurring in ETGs depends on their mass and density. It is early, short and intense in massive (and high density) ETGs and long, less efficient, and perhaps in bursts, in the low-mass (and low-density) ones. The key question to address and answer is: under which physical conditions either a single prominent episode or several episodes of star formations do occur? Which model best explains the whole pattern of observational data for ETGs? The hierarchical or the monolithic one? Or a complex combination of the two? Standard semi-analytical galaxy models are not suited to the aim, because they already contain the answer built in. Numerical NB-TSPH simulations are indeed the right tool to use, provided they include accurate treatments of important physical processes such as star formation, heating by energy deposit, cooling by radiative processes, chemical enrichment, etc., and finally suitable initial conditions.

2. Physical ingredients of the model galaxies

In general, a galaxy is made of DM, gas and stars. In the so-called NB-TSPH view, each component is represented by a number of particles (bodies) with different properties. Furthermore, galaxies are framed in a cosmological context for which some description is required and evolve with time, i.e. change their properties due to a large variety of physical

Table 1. Properties of the NB-TSPH models at the last computed stage of their evolution. Left to right: redshift z_f of the last computed model, age t_f at the same stage, total stellar mass M_s , total mass of the virialized halo M_{vir} , fraction of the total mass composed by star M_s/M_{vir} , fraction of the initial gas converted into stars $M_s/M_{g,i}$, virial radius r_{vir} of the whole system (i.e. stars, Dark Matter and gravitationally bound gas; it is the radius at which the mass density is 200 times the background density at the epoch of virialization, which roughly occurs for all models at about 2 Gyr, half mass radius $r_{s,1/2}$, of the stellar system projected on the XY plane, axis ratios b/a_{XY} of the stellar system projected on the XY plane. Times are in Gyr, masses in solar units M_\odot , and radii in kpc.

Model	z_f	t_f	M_s	M_{vir}	M_s/M_{vir}	$M_s/M_{g,i}$	r_{vir}	$r_{s,1/2}$	b/a_{XY}
HDHM	0.22	11.0	7.5×10^{11}	1.5×10^{13}	0.050	0.26	153.0	15.6	0.56
IDHM	0.77	8.0	7.4×10^{11}	1.5×10^{13}	0.050	0.26	141.8	16.5	0.48
LDHM	0.50	8.7	7.3×10^{11}	1.5×10^{13}	0.049	0.25	133.8	15.8	0.57
VLDHM	0.83	6.6	6.3×10^{11}	1.3×10^{13}	0.048	0.22	112.5	11.2	0.52
HDIM	1.00	5.8	2.0×10^{10}	2.1×10^{11}	0.100	0.45	37.6	5.7	0.62
IDIM	0.75	7.0	1.9×10^{10}	2.1×10^{11}	0.080	0.43	35.7	5.8	0.63
LDIM	0.58	8.1	1.9×10^{10}	2.0×10^{11}	0.100	0.42	33.3	5.2	0.75
VLDIM	0.15	11.8	1.7×10^{10}	1.4×10^{11}	0.120	0.38	28.3	4.9	0.83
HDLM	0.36	9.7	1.5×10^8	3.3×10^9	0.045	0.19	9.2	2.3	0.74
IDLM	0.22	11.0	1.4×10^8	3.3×10^9	0.040	0.16	10.0	2.4	0.67
LDLM	0.05	13.0	1.4×10^8	3.2×10^9	0.040	0.19	11.8	2.1	0.79
VLDLM	0.00	13.7	1.0×10^8	3.0×10^9	0.030	0.10	10.5	2.7	0.65

processes. The three components interact each other by gravity, whereas gas undergoes some special effects caused by sources and sinks of energy, e.g. radiative cooling and inverse Compton effect, heating by stellar feedback (supernova explosions, and stellar winds), and the cosmic UV background. Furthermore, the gas may undergo star formation, and chemical enrichment due to nuclear processing in stellar interiors, and mixing with stellar ejecta (supernovae and stellar winds).

Extremely large ranges in physical values of the physical properties of a galaxy are possible. In brief, galaxy masses go from 10^6 to $10^{14} M_\odot$ (8 orders of magnitude), gas temperature from 10 to 10^8 K (7 orders of magnitude), gas density from 10^{-33} to 10^{-18} g/cm³ (25 orders of magnitude), distances from 1 to 10^7 pc (7 orders of magnitude), and evolutionary time scales from 1 to 10^{10} years (10 orders of magnitude).

To suitably describe a galaxy with the NB-TSPH technique, very large numbers of particles are (would be) needed. For instance for baryonic mass of a galaxy of $10^{11} M_\odot$ (typical medium size object), the typical mass of

the BM particle is about $10^4 M_\odot$ whereas for a small size object with mass of $10^6 M_\odot$, the mass of the BM particle goes from 10^4 to $10^2 M_\odot$. Often the mass resolution is lower than those limits. Finally, galaxies may be the site of extremely violent phenomena, such as the supernova explosions, supersonic turbulence and shocks, and AGN feedbacks.

In the following, we will focus the attention only on the initial conditions, the star formation efficiency, and the treatment of the interstellar medium (ISM), leaving aside all other physical aspects of NB-TSPH simulations of models galaxies. The details about the sources of heating, the cooling mechanisms, the chemical evolution of the gas, etc. can be found in Merlin & Chiosi (2006, 2007); Merlin (2009); Merlin et al. (2010, 2012).

Initial Conditions. We adopt the so-called Λ CDM concordance model characterized by the parameters $H_0 = 70.1$ km/s/Mpc, $\Omega_\Lambda = 0.721$, $\Omega_b = 0.046$, baryon ratio 0.1656, $\sigma_8 = 0.817$, and index of the power spectrum of initial perturbations $n=0.96$. With the aid of this and the public code COSMIC by Berschinger (1995), we calculate the initial comoving posi-

tions and initial peculiar velocities of all particles at the time the highest density perturbation in the field exits the linear regime. Therefore, the kind of DM proto-haloes that are in place at each redshift are known. Instead of searching inside a large scale simulation, the perturbation (proto-halo) best suited to our proposes, we simply suppose that a perturbation of this type is there and derive with COSMIC the position and velocities of the DM+BM particles from a smaller area of the large scale field around the perturbation we are interested in.

The box has a size of $l=9.2$ comoving Mpc, and is described by grid of 463 particles. In this box, we impose a constrained density peak to induce a virialized structure at the center; build a gaussian spherical over-density with average linear density contrast $\delta\rho=b$ (with $b=3, 5, 10$) smoothed over a region of 3.5 comoving Mpc. COSMICS returns the initial comoving positions and peculiar velocities at the moment in which the particle with the highest density is exiting the linear regime. These cosmological simulations have been used to derive the initial conditions for a number of proto-galaxies at varying the mass and initial density of the (the cosmological density contrast of the proto-halo). For all details see Merlin et al. (2012).

In view of the discussion below, there is point to emphasize in relation to the gas density at which star formation is supposed to occur. The cosmological mixture of DM and BM in the proto-halo of mass $M_h = M_{DM} + M_{BM}$, where $M_h \simeq M_{DM}$, and radius R_h collapses when the density contrast with respect to the surrounding reaches a suitable value given by

$$\rho_h \equiv \left[\frac{3M_h}{4\pi R_h^3} \right] \geq \lambda \rho_u(z) \quad (1)$$

where $\rho_u(z) \propto (1+z)^{-3}$ is the density of the Universe at the redshift z , and λ the factor for the density contrast of the DM halo. The factor λ depends on the cosmological model of the Universe (see Bryan & Norman 1998, for all details). During the collapse, DM and BM are drag together to higher and higher densities and only when the gas density exceeds a threshold value, $\rho_g > \rho_g^*$, star formation is supposed to start. Therefore during the overall col-

lapse, BM matter under the action of radiative cooling may reach densities much higher than those reached by the dissipation-free DM. In other words the volume occupied by the bulk of gas and subsequently stars, can be much smaller than that of DM. The immediate consequence of it is that the initial dimensions of the proto-halo will not correspond to those of the stellar component built inside. All this will affect the final MRR of galaxies (see below). This allows us to evaluate the effect of local initial density, i.e. the density of BM (gas and/or stars) resulting from BM (gas) cooling inside the DM potential well. We name this the local initial density to distinguish it from the cosmological density at which the collapse of the proto-halo begins.

Star formation. This is modeled by means of the stochastic method proposed by Churches, Nelson, & Edmunds (2001) and Lia, Portinari, & Carraro (2002). First, only gas particles belonging to convergent flows (i.e. $\nabla \cdot v < 0$) and denser than the threshold density $\rho_g^* = 5 \times 10^{-25} \text{ g/cm}^3$ are considered eligible to form stars. No restriction on the temperature is imposed because thermal instabilities can produce star forming sites even within high temperature gas. If a gas particle satisfies these criteria, it is assumed to form stars at the rate

$$\frac{d\rho_s}{dt} = \epsilon_{sf} \frac{\rho_g}{t_{ff}} \quad (2)$$

where $t_{ff} \simeq 0.5/\sqrt{G\rho_t}$ is the free-fall time, ρ_t the local total mass density (DM plus BM), and ϵ_{sf} the dimensionless efficiency of the star formation process. This means that a gas particle is expected to turn a fraction ϵ_{sf} of its mass into stars over its free-fall time scale. However, a stochastic description of the star forming process is adopted to avoid the creation of an exceedingly large number of star particles. Thus, gas particles undergo a Monte Carlo selection to check whether or not they will actually form stars, in such a case they are instantaneously turned into collision-less star particles (see also Lia, Portinari, & Carraro 2002; Merlin 2009).

Empirical estimates of the efficiency of star formation based on observational data of star forming events inside the molecular clouds in

the local vicinity yield $\epsilon_{sf} \approx 0.025$ (Lada & Lada 2003; Krumholz & McKee 2007). In this case the gas density and free-fall time scale of are those of the cold molecular clouds. However, for the large scale star formation mechanism in a galaxy, the above estimate may not correspond to reality. As a matter of facts, considering that a typical galaxy with $10^{11} M_{\odot}$ mass in stars has to disposal a time scale of about 13 Gyr to build up its stellar content, the mean estimate of the star formation efficiency is closer to 0.1 rather than 0.02. The new estimate would increase by nearly a factor of ten if the time to disposal to form stars is much shorter than 13 Gyr, say 1 to 2 Gyr (as suggested by the age of the bulk of stars in many ETGs). In addition to this, it is not known whether ϵ_{sf} remained constant during different cosmic epochs due to the different mechanisms that form stars in metal-poor regions at high redshifts and in the molecular clouds of the local pool. Finally, it is not known whether the efficiency of star formation is the same in all galaxies independently of their mass (either total or baryonic). For all these reasons, we prefer to adopt here $\epsilon_{sf} = 1$, i.e. the process of star formation occurs at 100% efficiency (this means that *all* gas particles satisfying the star forming criteria will turn their total mass into stars within a free-fall time scale). The main motivation stands on the following considerations. Several numerical simulations calculated with different values of ϵ_{sf} clarify that within a certain range of values, the SFHs of the models with small values of ϵ_{sf} are apparently quite similar to those with $\epsilon_{sf} = 1$, the only difference being that small values of ϵ_{sf} lead to much more time-consuming simulations. The reason is that dense and cold clumps of matter, interacting with hotter material heated up by nearby SN explosions, require extremely small time-steps. In contrast, if the gas can easily form stars, this critical situation is avoided, and the simulations proceed much faster. The weak impact of ϵ_{sf} on the final SFH can be attributed to the self-regulation cycle between star formation and energy feedback. A high star formation efficiency implies a strong and sudden burst of stellar activity; but young stars soon pressurize their surroundings via energy feed-

back, quenching the formation of new stars. However, if the gas is sufficiently dense, radiative cooling is effective and further star formation can soon take place (positive feedback). With a low efficiency, fewer stars can form. Their heating is consequently lower, and more stars can soon form *before* feedback could halt the whole process. This ultimately leads to the same situation as in the previous case, with perhaps the minor consequence of a delayed enrichment in heavy elements of the medium. Clearly, other parameters play a more important role; for example, the density threshold ρ_* and the efficiency of feedback. Therefore the choice $\epsilon_{sf}=1$ and likely fast calculations is the best compromise. However, one should always keep in mind that adopting $\epsilon_{sf}=1$ may have other consequences on the dynamical evolution of the systems, favouring the collision-less collapse instead of the dissipative one.

Interstellar Medium: ROBO and MaNN. The thermodynamical and chemical treatment of the ISM in NB-TSPH simulations are difficult to model. Grassi et al. (2011a,b) proposed a method to include the ISM in NB-TSPH simulations and to get the cooling rate as a side self-consistent product. The idea is as follows: at a given time, the physical conditions of "a unit volume" of the ISM made of gas and dust in arbitrary proportions are specified by a pattern of parameters such as temperature, density chemical compositions etc., i.e. a point in the hyper-space of these parameters. After a certain amount of time has elapsed, the same volume has evolved to another state characterised by another pattern of same parameters, i.e. another point of the above hyper-space. We may picture this as a displacement vector. Consequently, if a large volume of this hyper-space is explored in advance, we would know at any arbitrary time all possible physical states in which the ISM can be found and the vector field of all possible displacements from the arbitrary initial stage to a final stage. In reality during its evolution, an elemental cell of the ISM will follow a path in the above hyper-space; at each step a final stage is the initial one of the next step and all are connected by the vector field. This view is particularly suited to implement the treatment of the ISM into

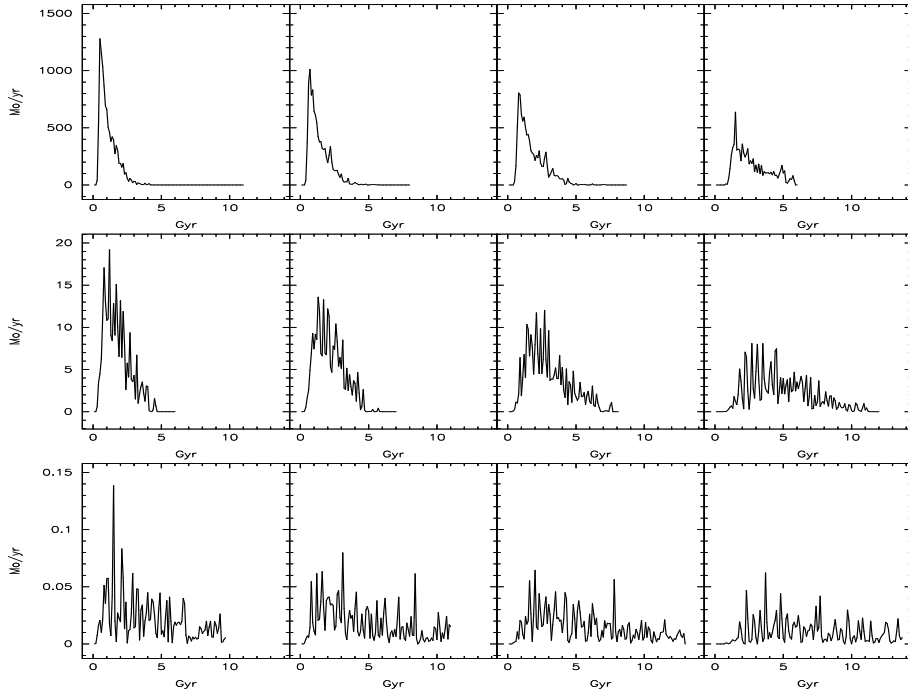


Fig. 1. Star formation histories for the reference models. Left to right: high density, intermediate density, low density, very low density. Top row: high mass; intermediate row: intermediate mass; bottom row: low mass.

NB-TSPH simulations provided that the vector field is taught in advance to a Multiple artificial Neural Network (MaNN). Given a "ISM particle of a NB-TSPH simulation, its current physical conditions are fed to the MaNN which restitutes the new physical conditions after a certain time interval. The evolution of the ISM is taken into account at a modest computational cost contrary to what it would be if the ISM evolution is incorporated into the NB-TSPH calculations. All details concerning the model of the ISM and the MaNN can be found in Grassi et al. (2011a,b); they are not repeated here for the sake of brevity.

3. NB-TSH galaxy models: results

Stirring baryons in the gravitational pot. The Duty Cycle between ISM and stars in a galaxy can be reduced to the following duty cycle: stars are born and evolve - stars inject energy and metals into the ISM by UV radiation, stel-

lar winds, and supernova explosions - gas heats up by energy injection and shocks and enriches in metals - gas cools down by radiative processes - gas collapses - new stars are born. The pot inside which all this occurs is the gravitational potential well. Therefore, the total galaxy mass and initial density are the key parameters. For all details see Chiosi & Carraro (2002), and Merlin et al. (2012).

Histories of Star Formation. At given initial over-density the models change their SFH from monolithic to bursting-like mode at decreasing total mass, whereas at given total mass the SFH changes from monolithic-like to bursting mode at decreasing initial over-density. This trend is shown in the various panels of Fig.1 and confirms the results found long ago by Chiosi & Carraro (2002). This basic dependence of the SFH on the total galaxy mass and initial over-density (environment) has been amply confirmed over the years by many observational and theoretical studies. It

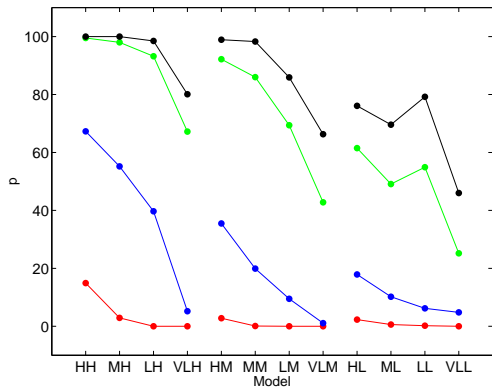


Fig. 2. Evolution of the mass assembly in the reference models. The X axis lists the models ordered as in Table 1 (the acronyms have been shortened for reasons of space), the Y axis displays the percentage p of assembled stellar mass at a given redshift z with respect to the $z = 1$ stellar mass; red: $z = 10$; blue: $z = 5$; green: $z = 2$; black: $z = 1.5$.

is worth noting here that this is possible only in monolithic-like scenarios.

Assembling the Stellar Mass. In the panels of Fig. 2 we show the gradual building up of the stellar mass of a galaxy as a function of the redshift. Remarkably the massive galaxies build up their stellar content earlier than those of smaller mass and also earlier than redshift $z = 2$.

Stellar ages. The distribution of the galactic ages ($T_{G,i}$) at which the star particles are created as a function of the radial distance is shown in Fig. 3 limited to the high and low mass models (the behaviour of the intermediate mass ones falls in between these two). The real ages of the star particles are $T_{*,i} = T_G - T_{G,i}$. In early epochs, the stars are preferentially created in the central regions, then the star forming activity expands to larger radii (inside-out mechanism), and moving towards the present time, the stellar activity tends to shrink again towards the centre. This simply mirrors the SFH and the mechanism of mass assembly presented above.

Mean metallicity. Turning now to the metal content reached by the model galaxies, we look at the average stellar metallicity as a function of the total stellar mass. The results

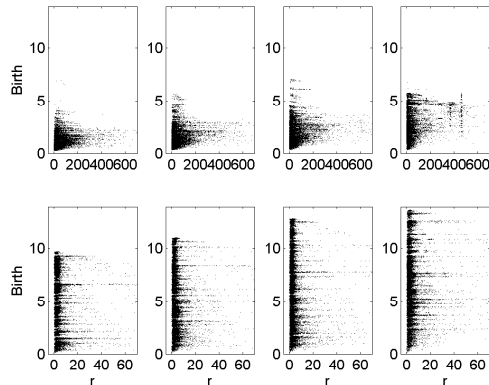


Fig. 3. Ages stars (in Gyr) as a function of their radial positions (distance from the barycenter in kpc) for the high (top row) and low mass models (bottom row) and decreasing density from left to right at the final time-step of their evolution. The radial distance is calculated from the barycenter of the stellar system (kpc). The virial radii of the stellar systems are similar to the extension along the X axis.

are shown in Fig. 4 where the red circles refer to all the star particles, whereas the blue ones only to those within the central 5 kpc of each model. The black lines are the median (solid) and the 16th and 84th percentiles (dashed) of the data presented in (Gallazzi et al 2005). Observational data and theoretical results agree only marginally. The absolute values of the theoretical metallicities are too low compared with the observational estimates, in particular for the most massive models which are almost an order of magnitude too metal-poor. This may be due to several factors:

- i) The theoretical values are straightforwardly computed averaging the metallicity of all particles within the galaxy radius without any further refinement, whereas the observational metallicity are *luminosity weighted*.
- ii) Use of different methods to obtain observational and theoretical metallicities.
- iii) The adopted IMF may not be suited to ETGs. For example, IMFs tailored to fit the solar vicinity (e.g. Kroupa), may underestimate the enrichment by massive stars in other environments. Recent studies seem to indicate that the IMF in mas-

sive ETGs is more skewed toward massive stars than commonly assumed (Cappellari et al. 2012) thus implying a net increase of metal production by massive stars in these systems.

- iv) The high star formation efficiency may play a role, favouring the formation of low metallicity stars at early times and reducing the average metallicity of the models.
- v) Finally, at least part of the observed color- (and hence metallicity-) mass relation might just be a spurious consequence of an aperture effect on the observational data (see Scodreggio 2001, for a detailed discussion).

In conclusion, considering that chemical enrichment in NB-TSPH simulations is still far from being fully satisfactory, we are inclined to say that theory and data marginally agree each other.

Metallicity gradients. Radial gradients in spectro-photometric properties of ETGs are known to exist (see e.g. La Barbera et al. 2010, 2011, and references therein), which are ultimately attributed to age and metallicity gradients of the constituent stellar populations (e.g. González 1993). To this aim, for each model galaxy, we calculate the median-binned metallicity profile, expressed as $\nabla_Z = d \log Z / d \log R$ over the radial interval $0.1 R_e$ to $1 R_e$. The gradient ∇_Z is calculated by applying three different weighting schemes, where each particle was assigned no-weight, mass-weighted, and luminosity-weighted. The results of Table 2 show that no significant differences exist within the errors, especially at the high mass end. Looking at the results in some detail, high-(low-) mass models exhibit metallicity gradients spanning the range from -0.4 (-0.02) to -0.27 (0.16), depending on the weighting scheme and environment. In general, low-density models tend to have more negative metallicity gradients. Moreover, at given density, high- (relative to low-) mass systems have more negative gradients.

Although the metallicities of our models do not match observations in an absolute sense, the relative variations of metallicity (between, e.g., different masses, and/or different galacto-

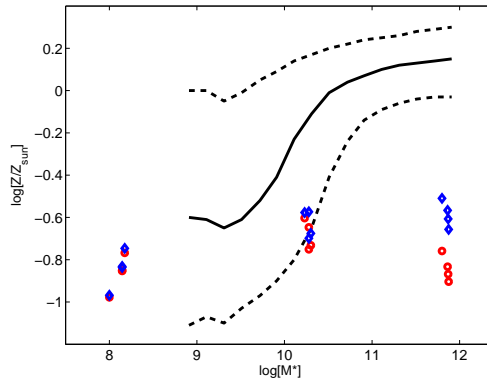


Fig. 4. Averaged metallicity $\log[Z/Z_{\odot}]$ versus stellar mass $\log M^* [M_{\odot}]$ for the twelve reference models, compared to the observed mass-metallicity relation. Black lines: data from Gallazzi et al. (2005) (solid line: median distribution of their sample; dashed lines: 16th and 84th percentiles). Red open circles: averaged metallicity of all stellar particles in each model. Blue open circles: averaged metallicity within the inner 5 kpc in each model.

centric distances) are likely more robust, as they are less dependent on the absolute calibration of the ingredients the models rely on. This motivates for a comparison of the predicted ∇_Z 's with observational results. A steepening of the metallicity gradient with galaxy mass, qualitatively consistent with that seen in our models, has been reported by La Barbera et al. (2010, 2011). For a galaxy mass of $3 \times 10^{11} M_{\odot}$ (similar to that of $\sim 7 \times 10^{11} M_{\odot}$ of models HDHM and LDHM), they estimate metallicity gradients of -0.37 ± 0.02 and -0.41 ± 0.02 for low- and high-density ETGs, respectively. At low density, the estimate of is fully consistent with our model predictions. At high-density, the models exhibit shallower gradients, by ~ 0.07 , in contrast to the data, where a (marginal) difference of -0.04 ± 0.03 is found. For what concerns low-mass models, they exhibit almost null gradients, consistent with the observational finding of Spolaor et al. (2009) that $\nabla_Z \simeq 0$ at a galaxy mass of $\sim 10^9 M_{\odot}$. Despite these results seem to indicate agreement between models and (some) available data-set, the whole subject is open to future investigation.

Table 2. Metallicity gradients of four ETG models in the radial range of $0.1 R_{eff}$ to $1 R_{eff}$. Column 1 is the model ID label. Columns 2, 3, and 4, correspond to cases where the ∇_Z is computed with no-weight, mass-weight, and luminosity-weight assigned to each particle. Errors are the rms of ∇_Z estimates among 100 projections of each model.

<i>ID</i>	∇_Z (no-weight)	∇_Z (mass-weighted)	∇_Z (lum-weighted)
(1)	(2)	(3)	(4)
LDHM	-0.39 ± 0.04	-0.40 ± 0.04	-0.33 ± 0.03
HDHM	-0.32 ± 0.04	-0.31 ± 0.04	-0.27 ± 0.03
LDLM	0.00 ± 0.04	$+0.01 \pm 0.02$	0.00 ± 0.06
HDLM	$+0.09 \pm 0.02$	-0.02 ± 0.01	0.16 ± 0.03

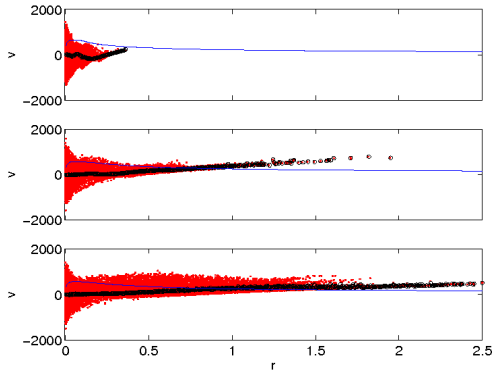


Fig. 5. Galactic winds in the HDHM model. Red points: radial velocities of gaseous particles (km/s) against the distance from the barycenter of the systems (Mpc). Black circles: mean radial velocity in the spherical shell at radius r . Solid blue line: escape velocity as a function of the radius. Top to bottom: $z = 4.4, 1, 0.2$.

Galactic Winds. Our models ejects conspicuous amounts of metal enrich gas in form of galactic wind over their whole history. In Fig. 5 we display the radial velocities of the gas particles in the case of HDHM model as a function of the radial distance at three different epochs and compare to the escape velocity (the blue solid lines; see the caption for more details). The mass of the ejected gas increases with time in all the models. The average velocity is proportional to the mass of the system, with massive galaxies generating winds at ≈ 2000 km/s, and low mass galaxies at about one tenth of this speed. Interestingly, the average radial velocity is proportional to the dis-

tance, like in a Hubble-like flow; the ejection of the gas is therefore an explosive phenomenon, rather than a slow outflow. However, looking more carefully it can be noticed that there are different linear velocities at the same radial distances, meaning that many explosive events have taken place. There is also a huge mass of gas moving outwards at slower speed, at late times (particularly in the HDHM model). The other model galaxies exhibit similar behaviour. Looking at the fractional amounts of escaping gas as a function of time – limited to the models HDHM, LDHM, HDLM, LDLM (the other models show similar behaviours) and once the system has virialized – the following trends are found. In the high mass realm, the fraction of gas *really* leaving the galaxy is only a few percent. On the contrary, in low mass systems more than half of the total gas has sufficient velocity to escape; Finally, the escaping gas is chemically enriched (see Merlin et al. 2012, for all details).

4. Mass density profiles

The geometrical structure of the model galaxies is best traced by the surface mass density profiles. To this aim, we choose the evolutionary stage at the redshift $z = 1$ and compare the surface mass density profiles of the model galaxies projected on the XY plane. These are plotted in Fig. 6 together with Sersic (1968) profile that best fits the model results,

$$\sigma_S(r) = \sigma_0 \times e^{(0.324-2m)\left[\left(\frac{r}{R_e}\right)^{1/m} - 1\right]} \quad (3)$$

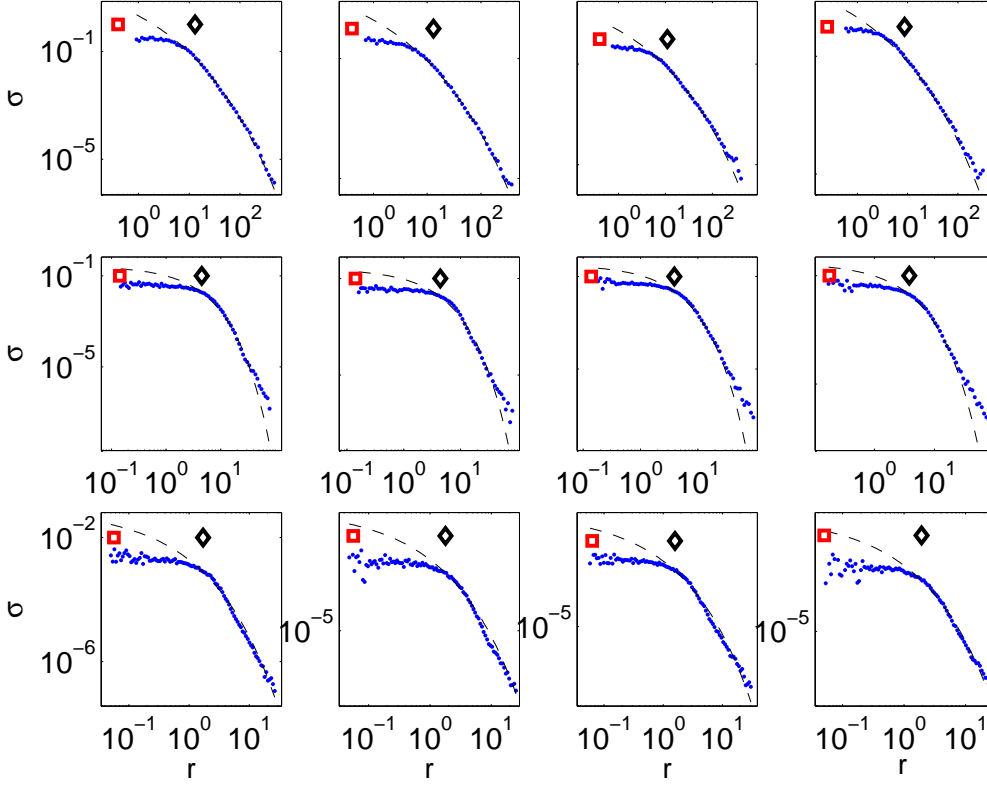


Fig. 6. Stellar surface density profiles for the reference models at the final time-step of each simulation. Plotted is the projected surface density σ [g/cm^2] against the logarithmic radius [kpc]. Blue dots: stellar particles radial averages; dashed line: best Sersic fit (see text for details). The black diamonds are placed at the effective radii R_e . The red squares are placed at the smallest value reached by adaptive softening lengths, thus indicating the effective resolution of the simulations. Left to right: high density, intermediate density, low density, very low density. Top row: high mass; intermediate row: intermediate mass; bottom row: low mass.

where R_e is the effective radius of the galaxy, as defined by Hernquist (1990), σ_0 the surface density at R_e , and m the Sersic index ($m = 4$ corresponds to the de Vaucouleurs profile). All profiles are computed starting at 0.2% of the virial radius of the galaxies to avoid the very central regions where softening may introduce spurious numerical effects. The best-fitting Sersic index is $m \sim 4$, $m \sim 1.5$, and $m \sim 2.5$, for high-, intermediate-, and low-mass models, respectively. In other words, high-(relative to low- and intermediate-) mass models tend to have higher m , in qualitative agreement with the existence of a luminosity-Sersic

index relation for ETGs (Caon, Capaccioli, & D’Onofrio 1993). However, one should notice that the most massive ellipticals in the local Universe tend to have $m \sim 8$ (e.g. Ferrarese et al. 2006), while we find $m \sim 4$. Moreover, our intermediate-mass models have somewhat lower m than the low-mass ones, which is only marginally consistent with luminosity- m relation, considering its large scatter.

The overall agreement between the models and the Sersic curves is good in the external regions. However, a clear departure from the expected fits is evident in all models at small radii (some fraction of R_e , indicated with the black

diamond shown in each panel). In the central regions, the model galaxies tend to *flatten out* their the mass density profile. Given the adaptiveness of the force softening, this feature can hardly be ascribed to numerical artifacts. Most likely, the high value of the dimensionless efficiency, $\epsilon_{sf} = 1$ we have adopted for the star formation rate, is the cause of it. This conclusion is strengthened by the three-dimensional mass density profiles compared with those by (Hernquist 1990) and (Navarro et al 1996, NFW), for stars and DM, respectively. While DM haloes smoothly follow the expected NFW profiles, the density of the stellar component never exceeds that of the DM, and contrary to the expectations (Padmanabhan et al. 2004), the central regions of the model galaxies are dominated by the DM, but the case of the HDHM model. The relations between the efficiency of star formation and the gas density at which star form is straightforward. If star formation proceeds slowly (low values of ϵ_{sf} , the gas can get high densities before it gets consumed by star formation itself. The opposite if star formation proceeds at high efficiency (high values of ϵ_{sf}). As a consequence of it, there is an immediate correlation between star formation and the dynamical behavior of a galaxy. Allowing gas particles to turn into stars as soon as they fulfill the required criteria ($\epsilon_{sf} = 1$) would produce extended stellar systems, with shallow potential wells and large effective radii. On the contrary, a low star formation efficiency leads to dense clumps of cold gas which yield more compact stellar systems (and to delay the onset of star formation).

Interestingly, this constrains the modality in which gas collapses and forms stellar systems. Historically, there are two possible and competing theoretical scenarios to describe the assembly of the stellar mass of an elliptical galaxy (excluding the possibility of merger events). In the first one, stars originally form far away from the effective radius of the galaxy and subsequently accrete onto its inner regions, in a non-dissipative fashion. In the other case, first the gas flows into the central regions and then it is turned into stars. If the correct scenario is the first one, smoothing of the central density cusp of the profiles is expected, be-

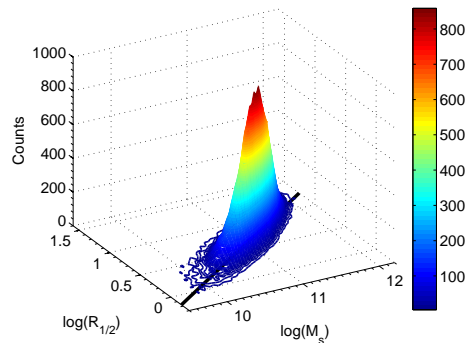


Fig. 7. 3D view of the MRR. The number frequency distribution of galaxies on the MR-plane: M_s is the total stellar mass in solar units and $R_{1/2}$ is the half-mass radius in kpc, and “Counts” is number of galaxies falling within each cell of the plane with dimensions $\Delta \log M_{12}=0.05$ and $\Delta \log R_{1/2}=0.05$. The data are from the HB sample of Bernardi et al (2010). The thick line on the MR-plane is the linear fit of the data: $\log R_{1/2} = 0.54 \log M_s - 5.25$.

cause the infalling stellar clumps loose orbital energy through dynamical friction and the halo heats up (Bertin, Liseikina & Pegoraro 2003). In the second case, the central distribution is expected to steepen up, because the gas radiates away its internal energy and an adiabatic contraction takes place (Gnedin et al. 2004). Obviously, both processes are expected to play a role in reality. This is indeed what we see in our models, in which however the final density profiles show a plateau in the central regions, as expected in the “infalling stars” model.

Our results clearly suggest that if stars are formed too early, the resulting stellar systems are too shallow, ending up in “wrong” profiles: stars will tend to conserve their velocity dispersion as they fall into the potential wells and will therefore have elongated orbits, which is not the case when gas is let dissipate part of its kinetic energy and reach very high densities before turning into stars.

In this context, it is worth recalling that there is some observational evidence for a deficit in the central luminosity of a few ETGs as recently found in observational data by Côté et al. (2007, their Fig. 1), and references therein). However, the observed flattening be-

gins at smaller radii (a fraction of R_e), and it is present only in bright (i.e. massive) systems, whereas the small systems seem to present a luminosity excess. Indeed, looking at the panels in the bottom row of Fig. 6, one can notice that the central profiles of low mass models show some scatter and tend to steepen in the very central regions (especially in the VLDM model). Recalling that the observational information stands on the luminosity profile, given the presence of young and hence luminous stellar populations in the cores of our low mass galaxy models, (and their absence in the cores of the massive ones), we can speculate that the trends of the observed curves should be fairly reproduced by translating the mass profiles into luminosity profiles. This is an interesting point, because the excess or deficit of light could be explained just in terms of the stars and DM orbits, without the presence of a super-massive black hole affecting the global dynamics in the center of the systems, as instead suggested in the studies quoted above.

5. The MRR of ETGs

In recent years, much attention has been paid to the MRR of galaxies, in particular the ETGs and the compact and passive ones at high z . The MRR is indeed basic to any theory of galaxy formation and evolution. The subject of the MRR of galaxies from ETGs to dwarf ellipticals and dwarf spheroidals, including also bulges and Globular Clusters, has been recently reviewed by Graham (2011) to whom we refer for many details. In addition to this, convincing evidence has been gathered that at relatively high redshifts, objects of mass comparable to that of nearby massive galaxies but smaller dimensions exist. These “compact galaxies” are found up to $z \geq 3$ with stellar masses from 10^{10} to $10^{12} M_\odot$ and half-light radii from 0.4 to 5 kpc (i.e. 3 to 4 times than more compact than the local counterparts of the same mass), and in nearly similar proportions there are galaxies with the same mass but a variety of dimensions (e.g., Mancini et al. 2009; Valentinuzzi et al. 2010), and bulge to disk ratios (e.g., Karim et al. 2011). However,

we will consider here only the case of standard ETGs, leaving the compact galaxies aside.

The key question to answer is: Why do ETGs obey a rather narrow MRR instead of scattering around showing a broader combination of masses and sizes? Spurred by this, we look for general physical principles governing this important scale relation. To clarify the aims and the methods of this study, we anticipate here the essence of our analysis. We speculate that the observed MRR for ETGs is the result of two complementary mechanisms. On one hand, the mass function of DM haloes hosting the visible galaxies gives (i) the typical cut-off mass at which, at any redshift, haloes become “common” on a chosen spatial scale, and (ii) the typical epoch at which low mass haloes begin to vanish at a rate higher than that at which they are born, because of merger events. On the other hand, these constraints define two loci (curves) on the MR-plane, because to each mass and formation redshift a typical dimension (i.e., radius) can be associated (using a basic relation between mass and radius of a collapsing object). If the typical dimension of a galaxy is somehow related to that of the hosting DM halo (as our NB-TSPH models seem to suggest), then the region of the MR-plane between the two limits fixed by the halo mass function is populated by galaxies whose dimensions are fixed at the epoch of formation, and only those objects that are “possible” at any given epoch may exist, populating a narrow region of the MR-plane.

The MRR of normal ETGs. The observational data we are considering is the HB sample selected by Bernardi et al (2010) from the SDSS catalogue, containing $\approx 60,000$ galaxies. The catalog contains the stellar mass M_s in M_\odot and the radius $R_{1/2}$ (in kpc) enclosing half of it. It worth clarify here that $R_{1/2}$ is nearly identical to the classical R_e . The linear fit of M_s and $R_{1/2}$ yields

$$\log R_{1/2} = 0.54 \log M_s - 5.25 \quad (4)$$

The slope and zero point of the above MRR are quite robust and coincide with previous determinations (Burstein, Bender, Faber, & Nothenius 1997; Chiosi & Carraro 2002; Shen et al. 2003; Graham 2011). It is worth noting

that toward the high mass end the slope of the MRR tends to increase to about 1, see Bernardi et al. (2010), Guo et al. (2009), van Dokkum et al. (2010), and Fig. 1 of Graham (2011). This is a point to keep in mind when interpreting the observational data.

Galaxy counts in the MR-plane. Before proceeding further it is worth looking at the number frequency distribution of galaxies with given mass and radius in the above SDSS sample. To this aim we divide the MR-plane in a grid of square cells with dimensions of 0.05 in units of $\Delta \log M_s / (10^{12} M_\odot)$ and $\Delta \log R_{1/2}$, and count the galaxies falling in each cell. In Fig. 7 we display the 3D space of these parameters to simultaneously highlight the distributions of the MRR along the direction parallel to the best-fit line on the MR-plane and the direction perpendicular to it. The view angle is chosen in such a way that the projections on the planes parallel and perpendicular to the MRR line can be easily figured out. While the projection on the plane parallel to direction of the best-fit line can be easily understood in terms of selection effects (galaxy mass fall-off at the high mass end and lack of data at the low mass end), the distribution perpendicular to this is more difficult to explain. Indeed *galaxies tend to fall in a rather narrow strip of the MR-plane, tightly gathering around the line with slope 0.54.*

Adding Dwarf galaxies. In addition to this we consider a small sample of dwarf galaxies of the Local Group to compare their location on the MR-plane with that of normal ETGs. The data for dwarf galaxies are from Burstein, Bender, Faber, & Nothenius (1997) and Woo et al. (2008). Dwarf galaxies are much more dispersed in the MR-plane and their mean MRR is $\log R_{1/2} = 0.3 \log M_s - 2.7$, which is much flatter than that of the normal ETGs.

Comparing Models with Data: The present day positions on the MR-plane of the reference of Table 1 and a few auxiliary models calculated for this purpose (see Chiosi et al. 2012, for all details) are shown in Fig. 8 together with the observational data. For the ancillary models suffice it to mention here that they are calculated for the intermediate and low mass galax-

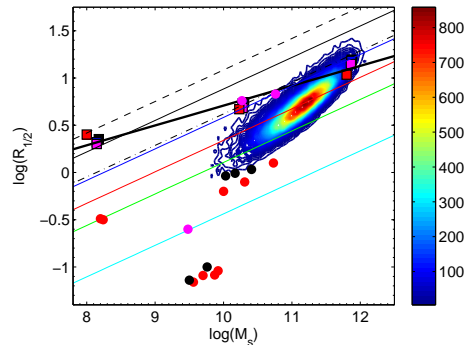


Fig. 8. Theoretical MRR, i.e. $\log R_{1/2}$ versus $\log M_s$. The filled squares are the reference models of Table 1 and the filled circles the ancillary models. The color code recalls the initial over-densities. However, as the entries of Tables 1 are fully sufficient to identify the models, the correspondence color-code-initial density is superfluous here. The thick black line is the fit of the reference models. The thin straight lines are the theoretical MRR on which proto-galaxies of given DM over-density settle down at the collapse stage as a function of the redshift. The lines are given by eqn. (5) from Fan et al. (2010): solid lines are for $m = 10$ and $f_\sigma = 1$; the color code indicates different redshifts (black: $z = 0$; blue: $z = 1$; red: $z = 2.5$; green: $z = 5$; cyan: $z = 20$); the thin black dashed line is for $m = 10$, $f_\sigma = 1.5$, and $z = 0$; Finally, the thin black dashed-dotted line is for $m = 5$ and $f_\sigma = 1$, and $z = 0$.

ies at varying either the collapse over-density or the star formation efficiency. Focussing on the reference models it is soon evident that only those of high (HM) and intermediate mass (IM) are consistent with the data. The low mass ones (LM) are too far off. It is worth recalling that these models have quit similar initial densities and initial redshifts. The slope of the theoretical MRR does not agree with the data. What does all this mean? To understand the issue we must clarify the correlation between initial over-density and present day position of the models, i.e. the correlation between the halo density, the SFH, and the present position on the MR-plane.

5.1. The filiation thread

Starting from the stage of proto-halo collapse eqn. (4) yields the initial MRR for the proto-haloes, whose slope is $R_h \propto M_h^{1/3}$ by construction. Inside this haies the BM, initially in form of gas, is gradually turned into stars, so that a new MRR is built up for the stellar content. In our case the one predicted by the NB-TSPH models.

The NB-TSPH reference and ancillary models allow us to clarify the different role played by the initial cosmological density contrast $\delta\rho_i(z)$ and the gas density $\rho_{g,sf}$ at the onset of star formation in determining the size of the resulting galaxy made of stars and the relation of between the initial gas mass and the final star mass. Further, the nature of the global process converting gas into stars.

Given the total mass oh the proto-halo M_h (it is worth recalling that $M_h \simeq M_{DM}$ so that they can be interchanged), the cosmological density $\delta\rho_i(z)$ determines the initial radial dimension of the DM perturbation. This does not coincide with the initial radius at which star formation begins in the baryonic component of a galaxy. In other words, within the potential well of DM, the gas keeps cooling at increasing density and only when the threshold density for star formation is met (which in turn is related to ϵ_{sf}), stars appear: the galaxy is detectable on the MR-plane. In this latter step of the filiation thread, $\rho_{g,sf}$ plays the dominant role. The remaining gas continues to fall into the gravitational potential well until either it is exhausted by SF or it is expelled via shocks because of energy feed back. Thanks to this there will be a correlation between the DM and the final mass in stars, measured by $m = M_{DM}/M_s$ (with $m \sim 10$ on the average).

NB-TSPH models (Merlin et al. 2012) indicate that the transformation of BM into stars occurs under the homology condition $GM_{DM}/R_{DM} \simeq GM_s/R_{1/2}$, i.e. equal gravitational potential energy per unit mass of the two components. In general, the model galaxies follow this rule and the two components of a galaxy lie on nearly parallel MRRs: i.e. $R_h \propto M_h^{1/3}$ and $R_{1/2} \propto M_s^{1/\beta}$ with $\beta \simeq 3$. At decreasing total mass, the exponent $1/\beta$ goes from

0.333 for galaxies with total mass $10^{13} M_\odot$ to about 0.2 for a mass of $10^9 M_\odot$ or even lower. This deviation from the $R_{1/2} \propto M_s^{1/3}$ law can be interpreted as due to an increasing departure from the condition of an ideal collapse because dissipative processes are now at work. The higher the initial mass, the closer the evolution of the proto-galaxy is to the simple collapse models. In other words, the straight collapse configuration corresponds to a minimum total energy of the system, whereas in all other cases the total energy system is far from the minimum level. Recasting the concept in a different way, the straight collapse is favored with respect to other energy costing configurations. Real galaxies tend to follow the rule by as much as they can compatibly with their physical conditions (total mass, initial density, SFH, ...). The result of it will be that the final model galaxies will be located on a new line (not necessarily a straight line but likely close to it) with a certain slope (about 0.2 in our case, see the linear fit of the final mean location of the reference models). The slope is flatter than the 0.33 slope of the iso-density line of the initial DM proto-galaxies. There is not reason for the two slopes being the same.

An analytical relationship. In the context of the Λ -CDM cosmology, Fan et al. (2010) have adapted the general relation (4) to provide an expression correlating the halo mass M_{DM} and the star mass M_s of the galaxy born inside it, the half light (mass) radius $R_{1/2}$ of the stellar component, the redshift at which the collapse takes place z_f , the shape of the BM galaxy via a coefficient $S_S(n_S)$ related to the Sersic brightness profile from which the half-light radius is inferred and the Sersic index n_S , the velocity dispersion of the BM component with respect to the that of DM (expressed by the parameter f_σ), and finally the ratio $m = M_{DM}/M_s$. The expression is

$$R_{1/2} = K \times \left(\frac{M_{DM}}{10^{12} M_\odot} \right)^{1/3} \frac{4}{(1+z_f)} \quad (5)$$

$$K = 0.9 \frac{S_S(n)}{0.34} \frac{25}{m} \left(\frac{1.5}{f_\sigma} \right)^2$$

Typical value for the coefficient $S_S(n_S)$ is 0.34. For the ratio $m = M_{DM}/M_s$, the empirical data

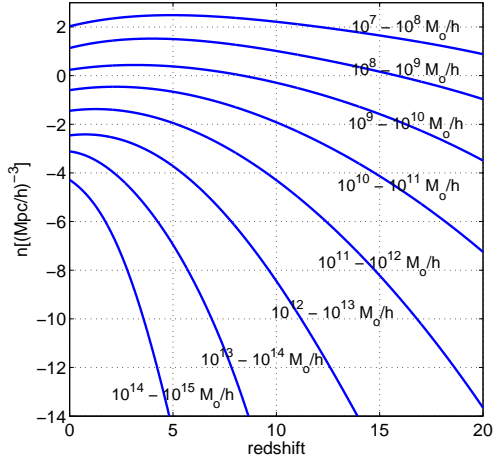


Fig. 9. The growth function of haloes $n(M_{DM}, z)$ reproduced from Lukic et al. (2007).

confine it in the range 20 to 40, whereas our NB-TSP models yield $m \approx 15$ to 20 depending on the particular case we refer to. For the purposes of the present study we take the rather low value $m = 10$. Finally f_σ yields the three dimensional star velocity dispersion as a function of the DM velocity dispersion, $\sigma_s = f_\sigma \sigma_{DM}$. Here we adopt $f_\sigma = 1$. For more details see Fan et al. (2010) and references therein and Chiosi et al. (2012). The slope of relation (5) is of course steeper but close to that of NB-TSH models; the difference can be fully ascribed to the complex baryon physics, which causes the stellar system to be slightly offset with respect to the locus analytically predicted from DM haloes. Therefore, a model slope different from that of the observational MRR (but still close to 0.3) is not the result of inaccurate description of the physical processes taking place in a galaxy. It is indeed remarkable that complicated numerical calculations clearly display this fundamental feature. *If this is the case, why do real galaxies gather along a line with a different slope?*

5.2. The cosmic galaxy shepherd

To answer the above question, we attack the problem from a different perspective, trying to investigate whether the observational MRR

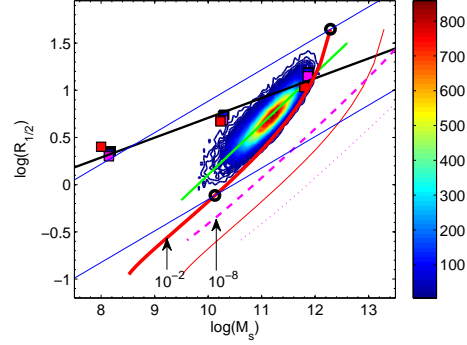


Fig. 10. The *cosmic galaxy shepherd* (CGS) and the corresponding locus of DM parent haloes (the red thick and thin solid lines, respectively) on the MR-plane. The halo number density is $N_h = 10^{-2}$ haloes per $(\text{Mpc}/h)^3$. For comparison, we also show the case for $N_h = 10^{-8}$ haloes per $(\text{Mpc}/h)^3$ (the magenta thick and thin dashed lines). The observational data is the HB sample of Bernardi et al (2010) with their linear fit (solid black line), and two theoretical MRR from eqn. (5) by Fan et al. (2010) (solid thin blue lines), relative to $z = 0$ and $z = 10$, with $m = 10$ and $f_\sigma = 1$ together with the reference galaxy models and their linear fit (filled squares and black solid line).

owes its origin to deeper reasons, likely related to the growth function of DM haloes (Lukic et al. 2007).

Given a certain number density of haloes N_h , on the $n(M_{DM}, z) - z$ plane of Fig. 9 this would correspond to an horizontal line intersecting the curves for the various masses at different redshifts. Each intersection provides a pair (M_{DM}, z) which gives the mass of the haloes fulfilling the constraint N_s at the corresponding redshift z . For any value N_h we get an array of pairs (M_{DM}, z) and with the aid the Fan et al. (2010) relationship (where the parameters m and f_σ are fixed) we can translated it into a relationship between the mass in stars and the half-mass radius of the baryonic galaxy associated to a generic host halo to be plotted on the MR-plane.

Repeating the procedure for other values of N_h , we get a manifold of curves on the MR-plane. It turns out that with $N_h = 10^{-2}$ haloes per $(\text{Mpc}/h)^3$, the curve is just at the edge of

the observed distribution. Higher values of the N_h would shift it to larger haloes (baryonic galaxies), the opposite for lower values of N_h . Why is $N_h = 10^{-2}$ haloes per $(\text{Mpc}/h)^3$ so special? Basing on crude, simple-minded arguments we recall that the total number of galaxies observed by the SDSS amounts to about $\approx 10^6$, whereas the volume of Universe covered by it is about $\approx 1/4$ of the whole sky times a depth of $\approx 1.5 \times 10^9$ light years, i.e. $\approx 10^8 \text{ Mpc}^3$, to which the number density of about 10^{-2} haloes per $(\text{Mpc}/h)^3$ would correspond¹. All this is shown in Fig. 10, where we also plot the curves relative to another possible choice $N_h = 10^{-8}$ haloes per $(\text{Mpc}/h)^3$, corresponding to 1 halo per $10^8 (\text{Mpc}/h)^3$, for the sake of comparison. It is an easy matter to see that the mean slope of the relation holding for $N_h = 10^{-2}$ haloes per $(\text{Mpc}/h)^3$ continuously varies from 0.5 to 1 and above as we move from the low mass to the high mass range. A similar trend for the slope is indeed also indicated by the observational data (see van Dokkum et al. 2010, and references therein). Owing to the many uncertainties we do not try to formally fit the median of the empirical MRR, but we limit ourselves to show that the locus predicted by the $N_h = 10^{-2}$ haloes per $(\text{Mpc}/h)^3$ falls on the MR-plane close to the observational MRR. Lower or higher values of N_h would predict loci in the MR-plane too far from the observational MRR unless other parameters of eqn. (5), e.g. m , are drastically changed assuming values that are difficult to justify.

Finally, we call attention on the fact the locus on the MR-plane defined by the solid curved line on the right panel of Figure (10) is ultimately related to the top end of the mass scale of haloes (and their filiated baryonic objects) that can exist at each redshift. In other words, it can be interpreted as the so-called cut-off mass of the galaxy mass distribution (see Lukic et al. 2007, for details and refer-

ences). We name this locus the *Cosmic Galaxy Shepherd* (hereafter CGS).

There are two points to be clarified. First, we have implicitly assumed that *each halo hosts one and only one galaxy and that this galaxy is an early type object matching the selection criteria of the Bernardi et al. (2010) sample*. In reality ETGs are often seen in clusters and/or groups of galaxies and many large spirals are present. Only a fraction of the total population are ETGs. One could try to correct for this issue by introducing some empirical statistics about the percentage of ETGs among all types of galaxy. Despite these considerations, to keep the problem simple we ignore all this and stand on the minimal assumption that each DM halo host at least one baryonic component made of stars. This is a strong assumption, on which we will come back again later on. Second, we have adopted $m = 10$ and $f_\sigma = 1$. According to Fan et al. (2010), the empirical estimate of M_{DM}/M_s ration is about 20-40, i.e. a factor of two to four less efficient star formation than we have assumed basing on our NB-TSPH models. However, a smaller value for m does not invalidate our analysis, because it would simply shift the location of the baryonic component on the MR-plane corresponding to a given halo number density. Finally, $f_\sigma = 1$ is a conservative choice. The same considerations made for m apply also to this parameter. At present, there is no need for other values.

Along the CGS, redshift and cut-off mass go in inverse order, i.e. low masses (and hence small radii) at high redshift and viceversa. This means that a manifold of MRRs defined by eqn. (5), each of which referring to a different collapse redshift, can be selected, and along each MRR only masses (both parent M_{DM} and daughter M_s) smaller than the top end are permitted, however each of which with a different occurrence probability: low mass haloes are always more common than the high mass ones. In the observational data, it looks as if ETGs should occur only towards the high mass end of each MRR, i.e. along the locus on the MR-plane whose right hand side is limited by the CGS. This could be the result of selection effects, i.e. (i) galaxies appear as ETGs only in

¹ We are well aware that this is a very crude estimate not taking into account many selection effects both in the observations and the halo statistics based on NB simulations, such as the Lukic et al. (2007) plane itself. However, just for the sake of argument, we can consider it as a good estimate to start with.

a certain interval of mass and dimension and outside this interval they appear as objects of different type (spirals, irregulars, dwarfs etc..), or (ii) they cannot even form or be detected (e.g. very extended objects of moderate/low mass). Finally, in addition to this, we argue that another physical reason limits the domain of galaxy occurrence also on the side of the low mass, small dimension objects.

Dissipation-less Collapse. It is an easy matter to figure out that the CGS is another way of rephrasing the top-hat spherical dissipation-less collapse for primordial fluctuations by Gott & Rees (1975) for which $R_{DM} \propto M_{DM}^{\frac{5+n}{6}}$ where n is the slope of the density fluctuation δ . Adopting $n = -1.8$, the power spectrum of CDM according to (Blumenthal 1984), we get the slope $d \log R_{DM} / d \log M_{DM} \simeq 0.53$ (Burstein, Bender, Faber, & Nothenius 1997, see also) The slope of the MRR derived from the dissipation-less collapse is the same of eqn. (4) all over the mass range from normal/giant galaxies down to classical Globular Clusters (Chiosi & Carraro 2002; Graham 2011, for more details). The advantage of the CGS is that it provides slope and zero point of the observational MRR and also predicts its change in slope at increasing star mass of the galaxy.

Given these premises, we suggest that the observational MRR represents the locus on the MR-plane of galaxies whose formation and evolution closely followed the scheme of dissipation-less collapse, i.e. the ones with mass close to the cut-off mass at each redshift.

5.3. Simulating the MRR

To sustain the above suggestion we try to simulate the observational MRR using the growth function calculated by Lukic et al. (2007) according to which the total number of the haloes that would nowadays populate the synthetic MR-plane and that should be compared with the observed galaxies are contained in the mass-bin $\Delta \log M_{DM}$ at redshift $z=0$. Prior to any other consideration one has to scale the theoretical predictions Lukic et al. (2007) that refer to a volume of space of 1 (Mpc/h)^3 , by a suitable factor N_{norm} to match the real vol-

ume covered by the data. Our sample contains about 60,000 galaxies, 6% of the total survey over a total volume of 10^8 Mpc^3 , therefore $N_{norm} = 5 \times 10^6$. To each mass M_{DM} expected at $z=0$ we must associate a redshift of formation in order to be able to estimate get the corresponding baryonic galaxy ($M_s, R_{1/2}$), by means of the Fan et al. (2010) relationship (of course assuming $m = M_{DM}/M_s$ and $f = \sigma_s/\sigma_{DM}$).

The growth functions of Lukic et al. (2007) allow us to derive the number of $N(M_{DM}, z)$ of haloes existing in each mass bin $\Delta \log M_{DM}$ at any redshift z . This number is the result of two competing effects: the formation of new haloes of mass M_{DM} via merger and/or acquisition of lower mass haloes, and the destruction of haloes of mass M_{DM} because of they merge to form higher mass haloes. Therefore

$$n(M_{DM}, z) = n(M_{DM}, z + \Delta z) + n_+(M_{DM}, z) - n_-(M_{DM}, z + \Delta z) \quad (6)$$

where n_+ and n_- represent the creation/destruction mechanisms. In particular, the quantity we are interested in is $n_+(M_{DM}, z)$, which is the number of new haloes of mass M_{DM} which are born at redshift z . The number of haloes that merge to form higher mass systems is in turn a fraction of the number of haloes existing at that time, i.e. $n_-(M_{DM}, z + \Delta z) = \eta \times n(M_{DM}, z + \Delta z)$, with $0 < \eta < 1$; so

$$n_+(M_{DM}, z) = n(M_{DM}, z) - (1 - \eta) \times n(M_{DM}, z + \Delta z) \quad (7)$$

The only free parameter here is η , the fraction of haloes that merge to form higher mass systems in the redshift interval Δz . In principle, the fraction η could vary with the redshift. However, for the sake of simplicity we assume that η remains constant. Thus, we obtain a value $N_+(M_{DM}, z)$ for each interval $M_{DM}, M_{DM} + \Delta M_{DM}$ and $z, z + \Delta z$. This number, re-normalized to unit over the whole interval, can be considered as the relative probability that a halo of mass M_{DM} is born at redshift

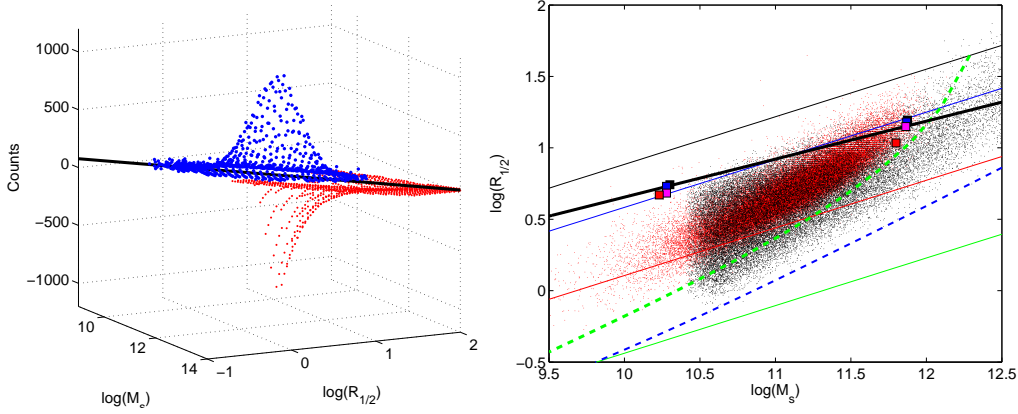


Fig. 11. Left Panel: Comparison of the theoretical (red dots, negative z -axis) with the observational (blue dots, positive z -axis) number frequency distributions of galaxies on the MR-plane: $\log M_s$ vs $\log(R_{1/2})$ (in M_\odot and kpc, respectively), “Counts” stands for $\Delta n(z) = n(z + \Delta z) - n(z)$, i.e. the number of haloes per Mpc^3 born between z and $z + \Delta z$. The thick line is the best fit of the observational data Bernardi et al (HB sample of 2010). The theoretical number frequencies have been plotted as negative quantities to get the mirror image of the observational data. Right Panel: Monte-Carlo simulation of the MRR: comparison of the theoretical (black dots) with the observational (red dots) distributions of galaxies on the MR-plane. The theoretical simulation is for $\eta = 0.01$. Superposed to it are the reference models (filled squares) for intermediate and high mass galaxies and their linear fit, and the CGS for $N_h = 10^{-2}$ haloes per $(Mpc/h)^3$ (the thick dashed green line is for the stellar component and the blue line for the DM halo). The thin trasverse lines are the Fan et al. (2010) relationships for different redshift, namely $z=0, 5, 10$, and 20 from the top to the bottom. Finally, the observational data are from Bernardi et al (2010).

z . Finally, for each halo of mass M_{DM} we compare a randomly chosen number $q \in [0, 1]$ with the cumulative probability

$$P_{z_i} = \sum_{z=z_{max}}^{z=z_i} n_+(M_{DM}, z)$$

until $q < P_{z_i}$, and take $z_f = z_i$ as its formation redshift. Using eqn. (5) we get the radius of the baryonic galaxy filiated by this halo to be plotted on the MR-plane. The distribution of galaxies on the MR-plane depends on the fraction η of haloes which merge to form higher mass systems in the redshift interval Δz . Only values of η smaller than about 0.02 lead to acceptable results. In the following we adopt $\eta = 0.01$. The predictions for $\Delta n(z) = n(z + \Delta z) - n(z)$ are shown in the left panel of Fig.11. The agreement is remarkable. In order to take into account that the observational sample contain a finite number of galaxies so that some cells of the theoretical MR-plane may not be populated in reality due to

stochastic effects we present Montecarlo simulations of the MR-plane using the Lukic et al. (2007) growth functions as probabilities. The resulting MRR is shown in the right panel of Fig. 11. We also look at the redshift (age) distribution of galaxies in the MRR: the vast majority of galaxies have been formed before redshift $z=1$. Finally, no correction is applied to the top end of the MRR to account for the fact several galaxies per halo could be found at this mass range (above say $M_s > 10^{12} M_\odot$. This would remove nearly all the object falling on the MRR at the high mass end, i.e. say above $10^{12} M_\odot$.

5.4. How many mergers?

Assuming for simplicity that η is constant with time, we calculate the ratio between the total number of merger events, $N_{merg} = \sum_{z_{bin}} \eta \times n(M_{DM}, z)$ and the total number of galaxies that

ever existed during the Hubble time, $N_{tot} = \sum_{z_{bin}} n_+(M_{DM}, z)$

$$\frac{N_{merg}}{N_{tot}} = \frac{\sum_{z_{bin}} \eta \times n(M_{DM}, z)}{\sum_{z_{bin}} n_+(M_{DM}, z)} \quad (8)$$

Crude calculations yield $N_{merg}/N_{tot} \simeq 0.10 - 0.15$ for $\eta = 0.01$. This percentage increases to about 50% for $\eta = 0.05$. With the latter value, the MRR is much more dispersed than the observational one. Therefore, it seems that only a fraction (from 0.1 to 0.5) of haloes should have merged during the whole history of the Universe. Owing to the many uncertainties still affecting the above discussion, we do not insist on this issue.

6. Conclusions

In this review we have reported on recent studies aimed at (i) exploring the properties of model galaxies for ETGs in the quasi monolithic or early hierarchical scenario in the Λ -CDM Universe, (ii) casting light on the origin of the star mass-radius relation of ETGs. In the adopted scenario, mergers of sub-structures made of DM and BM are on purpose let occur early on during the lifetime of a galaxy, in order to check whether the resulting object may account for the properties of real ETGs without invoking major merger during the the whole life of a galaxy.

The key result is that the SFH is driven by the total mass of the system, the initial over-density with respect to the surrounding medium, and the threshold density inside the gravitational potential well reached by BM gas at the onset of star formation. In brief: (i) At given initial over-density, and star forming efficiency (ϵ_{sf}), the model galaxies SFH from monolithic to bursting-like mode at decreasing total mass (from big ETGs to small ETGs); (ii) at at given total mass the SFH changes from monolithic-like to bursting mode at decreasing initial over-density, and in addition to this the peak of stellar activity is gradually shifted toward the present (downsizing); (iii) at given total mass and initial over-density, the efficiency of star formation (the threshold gas density to) adds another dimension to the problem in tuning the kind of star formation history taking

place in a galaxy in between the two paradigm behaviour above and the some how determining the mean dimensions of galaxy component made of stars: large for high efficiencies and relatively small for low efficiencies. Finally, the models of high mass galaxies complete their mass assembly and star formation at redshifts larger than 2, The structural properties of the model galaxies (surface mass density profiles of BM and DM) nicely agree with the current information on these quantities. Galactic winds are about 10 % to 50% of the gas mass in massive and low mass galaxies, respectively. This material is significantly enriched in metals. The mean metallicity and the metallicity gradients are in marginal agreement with current observational data.

The MRR of ETGs stems from the action several concurring factors: (i) the CGS visualizing the cut-off mass of the galaxy mass distribution at each redshift. It is set by the cosmic growing of gravitationally bounded density perturbations and associated $N(M_{DM}, z)$. The slope of the CGS goes from 0.5 to 1 as the mass increases. It is reminiscent of the slope of the MRR for dissipation-less collapse. (ii) The manifold of lines of equal initial density but different redshift along which pro-haloes of any mass crowd (slope of this mass-radius relation is $1/3$ by construction). (iii) given the initial density, collapse redshift, and star formation efficiency, the proto-haloes of different mass filiate baryonic galaxies with certain values of M_s and $R_{1/2}$ at the present time. The baryonic galaxies crowd along mass-radius relations whose slope changes from 0.3 to 0.2 or less as the galaxy mass (either total or stellar) decreases. The MRR for ETGs is locus on which the manifold of mass-radius relations on which the BM galaxies of any mass would lie intersect the CGS. The galaxies at the intersection are close to the cut-mass and evolve in condition closely following the dissipation-less collapse. They trace the MRR of ETGs we observe today.

Acknowledgements. C.C. is grateful to all collaborators U. Buonomo, G. Carraro, T. Grassi, C. Lia, E. Merlin, S. Pasetto, L. Piovan, and R. Tantalo who all contributed with enthusiasm and dedication to develop the subject of galaxy formation and evolu-

tion at the Padova University. Finally, C.C. likes to thanks Drs. F. Combes, R. Buonanno, and G. Bono for inviting him to attend the conference and deliver this plenary lecture.

References

- Bernardi, M., et al. 2010, *MNRAS*, 404, 2087
 Bertin, G., Liseikina, T., & Pegoraro, A. 2003, *A&A*, 405, 73
 Bertschinger, E. 1995, *astro-ph/9506070*
 Blumenthal, G. R., et al. 1984, *Nature*, 311, 517
 Bryan, G. L., & Norman, M. L. 1998, *ApJ*, 495, 80
 Burstein, D., Bender, R., Faber, S., & Nolthenius, R. 1997, *AJ*, 114, 1365
 Caon, N., Capaccioli, M. & D'Onofrio, M. 1993, *MNRAS*, 265, 1013
 Cappellari, M., et al. 2012, *Nature*, 484, 485
 Chiosi, C., & Carraro, G. 2002, *MNRAS*, 335, 335
 Chiosi, C., Merlin, E., & Piovan, L. 2012, *astro-ph:1206.2532*
 Churches, D. K., Nelson, A. H., & Edmunds, M. G. 2001, *MNRAS*, 327, 610
 Côté, P., et al. 2007, *ApJ*, 671, 1456
 van Dokkum, P. G., et al. 2010, *ApJ*, 709, 1018
 Fan, L., et al. 2010, *ApJ*, 718, 1460
 Ferrarese, L., et al. 2006, *ApJS*, 164, 334
 Gallazzi, A., et al. 2005, *MNRAS*, 362, 41
 Gnedin, O. Y., et al. 2004, *ApJ*, 616, 16
 González, J. J. 1993, Line strength gradients and kinematic profiles in elliptical galaxies, PhD Thesis, University of California, Santa Cruz, USA
 Gott, III, J. R. and Rees, M. J. 1975, *A&A*, 45, 365
 Graham, A. W. 2011, *ArXiv*, e-prints: 1108.0997
 Grassi, T., et al. 2011, *A&A*, 533, A123
 Grassi, T., et al. 2011, *ArXiv*, e-print: 1103.0509
 Guo, Y., et al. 2009, *MNRAS*, 398, 1129
 Hernquist, L. 1990, *ApJ*, 356, 359
 Karim, A., et al. 2011, *ApJ*, 730, 61
 Krumholz, M. R., & McKee, C. F. 2007, *ApJ*, 630, 250
 La Barbera, F., et al. 2010, *AJ*, 140, 1528
 La Barbera, F., et al. 2011, *ApJ*, 740, L41
 Lia, C., Portinari, L., & Carraro, G. 2002, *MNRAS*, 330, 821
 Lada, C. J., & Lada, E. A. 2003, *ARA&A*, 41, 57
 Lukić, Z., et al. 2007, *ApJ*, 671, 1160
 Mancini, C., et al. 2009, *A&A*, 500, 705
 Merlin, E., & Chiosi, C. 2006, *A&A*, 457, 437
 Merlin, E., & Chiosi, C. 2007, *A&A*, 473, 733
 Merlin, E. 2009, Simulating the formation and evolution of galaxies. Methods and results, PhD Thesis, University of Padova, Italy
 Merlin, E., et al. 2010, *A&A*, 513, A36
 Merlin, E., et al. 2012, *ArXiv* e-prints: 1204.5118
 Navarro, J. F., Eke, V. R., & Frenk, C. S. 1996, *MNRAS*, 283, L72
 Padmanabhan, N., et al. 2004, *Nature*, 9, 329
 Scodreggio, M. 2001, *AJ*, 121, 2413
 Sersic, J. L. 1968, Atlas de galaxias australes (Observatorio Astronomico, Cordoba, Argentina)
 Shen, S., et al. 2003, *MNRAS*, 343, 978
 Spolaor, M., et al. 2009, *ApJ*, 691, L138
 Tortora, C., et al. 2010, *MNRAS*, 407, 144
 Tremonti, C. A., et al. 2004, *ApJ*, 613, 898
 Valentinuzzi, T., et al. 2010, *ApJ*, 712, 226
 Woo, J., Courteau, S., & Dekel, A. 2008, *MNRAS*, 390, 1453